

Article

Radiolabeled Risperidone microSPECT/CT Imaging for Intranasal Implant Studies Development

Jon Ander Simón¹, Emilia Utomo², Félix Pareja¹, María Collantes^{3,*}, Gemma Quincoces¹, Aarón Otero³, Margarita Ecay³, Juan Domínguez-Robles^{2,4}, Eneko Larrañeta^{2,*} and Iván Peñuelas^{1,3}

¹ Radiopharmacy Unit, Department of Nuclear Medicine, Clinica Universidad de Navarra, University of Navarra, IdiSNA, 31008 Pamplona, Spain

² School of Pharmacy, Queen's University Belfast, Lisburn Road 97, Belfast BT9 7BL, UK

³ Translational Molecular Imaging Unit (UNIMTRA), Department of Nuclear Medicine, Clinica Universidad de Navarra, 31008 Pamplona, Spain

⁴ Department of Pharmacy and Pharmaceutical Technology, University of Seville, 41012 Seville, Spain

* Correspondence: mcollant@unav.es (M.C.); e.larrañeta@qub.ac.uk (E.L.)

Abstract: The use of intranasal implantable drug delivery systems has many potential advantages for the treatment of different diseases, as they can provide sustained drug delivery, improving patient compliance. We describe a novel proof-of-concept methodological study using intranasal implants with radiolabeled risperidone (RISP) as a model molecule. This novel approach could provide very valuable data for the design and optimization of intranasal implants for sustained drug delivery. RISP was radiolabeled with ¹²⁵I by solid supported direct halogen electrophilic substitution and added to a poly(lactide-co-glycolide) (PLGA; 75/25_{D,L}-Lactide/glycolide ratio) solution that was casted on top of 3D-printed silicone molds adapted for intranasal administration to laboratory animals. Implants were intranasally administered to rats, and radiolabeled RISP release followed for 4 weeks by in vivo non-invasive quantitative microSPECT/CT imaging. Percentage release data were compared with in vitro ones using radiolabeled implants containing either ¹²⁵I-RISP or [¹²⁵I]INa and also by HPLC measurement of drug release. Implants remained in the nasal cavity for up to a month and were slowly and steadily dissolved. All methods showed a fast release of the lipophilic drug in the first days with a steadier increase to reach a plateau after approximately 5 days. The release of [¹²⁵I]I⁻ took place at a much slower rate. We herein demonstrate the feasibility of this experimental approach to obtain high-resolution, non-invasive quantitative images of the release of the radiolabeled drug, providing valuable information for improved pharmaceutical development of intranasal implants.

Keywords: intranasal implant; molecular imaging; SPECT/CT; risperidone; radioiodination



Citation: Simón, J.A.; Utomo, E.; Pareja, F.; Collantes, M.; Quincoces, G.; Otero, A.; Ecay, M.; Domínguez-Robles, J.; Larrañeta, E.; Peñuelas, I. Radiolabeled Risperidone microSPECT/CT Imaging for Intranasal Implant Studies Development. *Pharmaceutics* **2023**, *15*, 843. <https://doi.org/10.3390/pharmaceutics15030843>

Academic Editors: Zhenjia Wang and Artur Turek

Received: 2 February 2023

Revised: 2 March 2023

Accepted: 2 March 2023

Published: 4 March 2023



Copyright: © 2023 by the authors. Licensee MDPI, Basel, Switzerland. This article is an open access article distributed under the terms and conditions of the Creative Commons Attribution (CC BY) license (<https://creativecommons.org/licenses/by/4.0/>).

1. Introduction

Implantable drug delivery systems are capable of providing sustained drug delivery over prolonged periods of time [1–6]. The interest in this type of system has been experiencing an increase over recent years due to its potential advantages over conventional drug delivery systems. Implantable systems can be used for either systemic or local drug delivery, with many advantages. First of all, once implanted, these devices are capable of providing unattended sustained drug delivery [7–9]. Therefore, patients are not required to rely on continuous and repeated oral intake of medication, which will improve patient compliance [7]. A wide variety of implantable drug delivery systems have been described, including subcutaneous implants [10–14], cardiovascular devices [15–21], or orthopaedic implants [22,23]. Among these type of implantable devices, intranasal implants have been described for local drug delivery [24]. These devices are normally applied within nasal sinuses after surgery to maintain sinus patency while releasing corticosteroids to reduce inflammation and reduce polyp recurrence [24].

Intranasal drug delivery has shown potential not only for treating local conditions but to administer drug systemically or even to achieve a more effective delivery of drugs into the brain [25,26]. Most of the formulations developed for intranasal delivery are liquid- or gel-based formulations [27–29]. The only type of implantable devices clinically available for intranasal applications are the previously mentioned nasal implants/stents for local drug delivery. Accordingly, there is a clear need for new types of implantable devices that combine the advantages of implantable devices and intranasal drug delivery.

As *in vitro* release kinetics might differ from *in vivo* forms, there is a real need for the development of advanced techniques to measure drug release from intranasal implants *in vivo*. Radionuclide-based non-invasive molecular imaging techniques are currently widely used in the clinical setting for diagnosis of multiple diseases and or pathophysiological altered conditions. In addition, their fully translational nature (“from bench to bedside and back”) has fostered the use either of positron emission tomography (PET) or single-photon emission computed tomography (SPECT) technologies in pharmaceutical development. These techniques can provide three-dimensional, fully quantitative, non-invasive, longitudinal, whole-body images with submillimeter resolution and an extremely high sensitivity that is unsurpassable by any other *in vivo* imaging technology, given that micro or nanomolar concentrations of radiolabeled molecules in tissues can be detected. In addition, the current state-of-the-art multi-technology devices adapted for small animal imaging combine high-resolution molecular imaging using microPET or microSPECT with anatomical imaging using computed tomography (CT).

The main potential drawback of these techniques is their much lower throughput as compared to others, their cost, and the need for special facilities for the use of radioactive material. However, their fully translational nature and their aforementioned unique characteristics could make them ideal for research, as in the case described in this work.

On the other hand, visible-light *in vivo* imaging techniques such as bioluminescence and fluorescence are widely available, relatively non-expensive, and can provide a high experimental throughput. However, they have several problems intrinsically bound to the physical nature of the wavelength of visible light photons, including those related with autofluorescence of biological tissues and mainly the lack of real 3D information as visible light photons are significantly absorbed by the tissues, and hence the exact location and intensity of a signal cannot be obtained. Furthermore, these techniques are intrinsically non-quantitative, and only magnitudes such as “relative light units” can be obtained, but there is no way to really obtain fully quantitative values.

This work describes a proof-of-concept study describing the use of intranasal implants for drug delivery using risperidone (RISP) as a model molecule. Applying solid-based radioiodination, we herein radiolabeled RISP with a long-lived radionuclide (^{125}I), designed poly(lactide-co-glycolide) (PLGA; 75/25 D,L -Lactide/glycolide ratio) (PLGA)-based intranasal microimplants adapted for administration to rats, loaded them with ^{125}I radiolabeled RISP, and *in vivo* imaged microimplants for a month using high-resolution MicroSPECT/CT.

2. Materials and Methods

2.1. Risperidone Radiolabelling

RISP (Enke Pharma-Tech Co., Ltd., Cangzhou, China) was radiolabeled by direct electrophilic substitution with ^{125}I (Figure 1) under oxidative conditions using a modified protocol derived from Saddar et al. [30]. Given the very low solubility of RISP in aqueous solvents, we used Iodination Beads (ThermoFischer Scientific, Waltham, MA, USA) to achieve mild oxidation conditions and permit a solid-supported reaction in a RISP powder suspension. The radionuclide was chosen on the basis of its long half-life and radioactive properties that could permit follow up of the release of the radiolabeled RISP for more than 1 month. ^{125}I has a half-life of 59.49 days, and it decays by electron capture to an excited state of ^{125}Te that immediately decays by emission of 35 keV gamma rays.

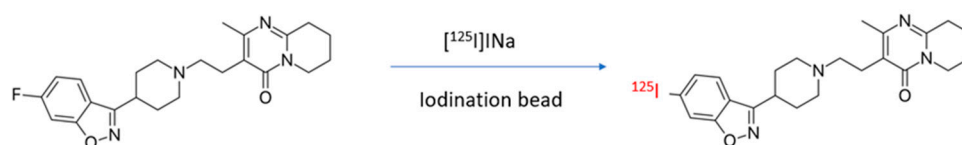


Figure 1. Solid supported ^{125}I -radiolabelling of RISIP via direct halogen electrophilic substitution.

For the radiolabeling reaction, one Pierce™ iodination bead was pre-wetted in 500 μL of PBS (pH = 6.5) for 5 min, removed from the solution, and dried over filter paper. Thirty milligrams of RISIP was weighted in a bottom-flat glass vial, and the iodination bead was added along with 300 μL of fresh PBS and 18,5 MBq of $^{125}\text{I}]\text{I}^-$ solution (Perkin Elmer Inc, Amsterdam, the Netherlands) in <5 μL . The suspension was thoroughly mixed by shaking and left with gentle magnetic stirring for ≈ 72 h.

2.2. Quality Control

The radiolabeling reaction was periodically monitored by radio thin-layer chromatography (radioTLC). For this purpose, samples were taken from the reaction vial just after increasing the stirring speed. Such samples (that contained both the non-dissolved RISIP and the reaction solution) were added into 10 μL of an acidified PBS solution (3 mL of HCl 1 M:2 mL of PBS) to dissolve RISIP, then seeded at 1 cm from the bottom of a 10 cm iTLC SG strip (Agilent Technologies, Santa Clara, CA, USA) that was developed to a final distance of 8 cm from the origin with 0.9% NaCl. Chromatograms were analyzed using a radioTLC scanner (Scam RAM, LabLogic, Sheffield, UK). The separation method had previously been validated by our group using non-radioactive RISIP and iodide samples visualized with a 7.5 g/L KMnO_4 , 50 g/L K_2CO_3 , and 0.625 g/L NaOH solution as described in the Section 3.

2.3. ^{125}I -Risperidone Extraction and Purification

At the endpoint of the reaction, the iodination bead was removed from the radiolabeling vial, the suspension was thoroughly mixed and transferred into an Eppendorf tube, the vial was washed twice with 200 μL of PBS, and the three samples were mixed. The overall reaction suspension was centrifuged at 9000 rpm for 1 min, and the supernatant was removed. The solid precipitate was then washed twice with 200 μL of PBS, and the supernatant was analyzed by radioTLC as described above to check for the absence of free $^{125}\text{I}]\text{I}^-$. The precipitate containing ^{125}I -labelled RISIP (^{125}I -RISIP) was then dried overnight with gentle shaking at 37 $^\circ\text{C}$ in a ThermoMixer C (Eppendorf Thermoshaker, Hamburg, Germany).

2.4. Preparation of Microimplants Containing ^{125}I -RISIP or $^{125}\text{I}]\text{I}^-$

To prepare PLGA-based microimplants, silicone molds were used (see Figure 2A,B). These implants were prepared by using a 3D-printed poly(lactic acid) and casting silicone on top as described previously (Figure 2C,D) [11]. The silicone (Xiameter® RTV-4250-S) (Notcutt, Surrey, UK) was prepared by mixing a silicone elastomer with a curing agent (ratio 10:1). The molds contained two parts: a part containing 3 cavities to prepare 3 implants and a lid. Viatel™ DLG 7509 E PLGA (75/25 D,L -Lactide/glycolide ratio; $M_n = 61.9$ kDa; $M_w = 104.2$ kDa; $T_g = 50$ $^\circ\text{C}$; ester end group) (Ashland Specialities Ireland, Mullingar, Ireland) was used to prepare implants. In order to achieve this, approximately 20 mg of the dry solid ^{125}I -RISIP mixture was dissolved in 70 μL of dichloromethane. Subsequently, 16 mg of PLGA was added to the ^{125}I -RISIP solution, and the solution was carefully mixed (to avoid bubble formation) for 20 min. Using the silicone mold and a positive displacement pipette, 15 μL of the ^{125}I -RISIP/PLGA mixture containing around 750 kBq was added to the silicone molds to prepare each microimplant. After 24 h at room temperature, microimplants were taken out from the molds, burrs were carefully removed and longitudinally cut in half, and their activity was measured in a dose calibrator calibrated for ^{125}I . Such halves contained 150–225 kBq ^{125}I and were rigid enough for intranasal in vivo administration. As controls

for in vitro and in vivo release studies, microimplants containing [^{125}I]INa were prepared in a similar way but using [^{125}I]INa instead of ^{125}I -RISP.

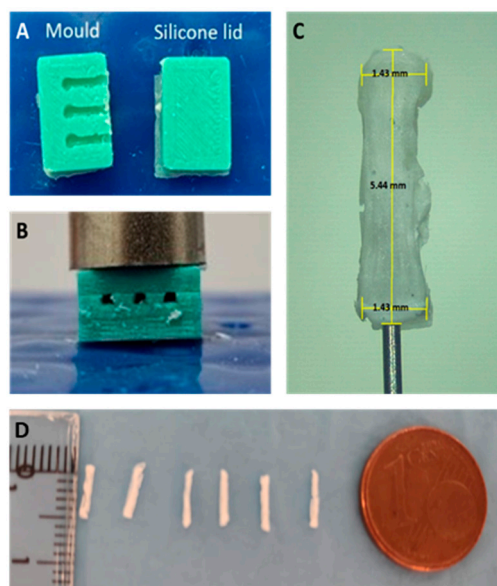


Figure 2. Images showing silicone molds used to prepare intranasal implants (A,B). Microscopy image of a PLGA implant prepared using the silicone molds (C). Size comparison of microimplants (D).

2.5. In Vitro Release Studies

Microimplants containing either ^{125}I -RISP or [^{125}I]INa were placed in 2 mL PBS at 37 °C with constant agitation (350 rpm) in a thermomixer. Five microliter triplicate samples were taken at defined time points for up to 30 days and radioactivity measured in a gamma counter (Hidex Automatic Gamma Counter, Turku, Finland) calibrated for ^{125}I , and percentage release ratios were calculated.

In parallel, the release of unlabeled RISP from PLGA implants in PBS (pH = 6.5) at 37 °C was evaluated using HPLC. For this purpose, an Agilent 1220 Infinity II LC gradient system (Agilent Technologies UK Ltd., Stockport, UK) equipped with a Phenomenex® SphereClone™ C18 ODS column (150 mm length × 4.60 mm internal diameter, 5 μm particle size) was used. The mobile phase contained a mixture of organic (85% *v/v*) and aqueous phases (15% *v/v*). The aqueous phase contained 10 mM sodium dihydrogen phosphate buffer. On the other hand, the organic phase contained a mixture of methanol and acetonitrile (75:25% *v/v*). RISP detection was carried out at 235 nm.

2.6. Animal Studies

Female Wistar rats (212 ± 22.5 g, Harlan Laboratories S.A., Barcelona, Spain) were used. Animals were socially housed on 12 h light–dark cycles under standard conditions in compliance with the current regulation and given free access to food and water.

2.7. Microimplant Intranasal Administration and In Vivo Release Studies

Radiolabeled microimplants halves (≈5.5 mm × 0.5 mm) were introduced into a 20 GA 1.1 mm × 30 mm i.v. catheter (Insyte Autoguard BC, BD medical, Madrid, Spain) previously cut at around 15 mm from the hub to flatten the bevel and shorten its length. A total of 7–10 mm of the catheter were slowly introduced through the nostril of anesthetized rats (2% isoflurane in 100% O₂ gas), the shaft was carefully pushed until the implant was left into the nasal cavity, and then the catheter was removed (Figure 3). Six animals were treated with ^{125}I -RISP microimplants, while three were treated with microimplants loaded with [^{125}I]INa as controls. The correct placement of the microimplants inside the nasal cavity was verified by microSPECT/CT imaging.

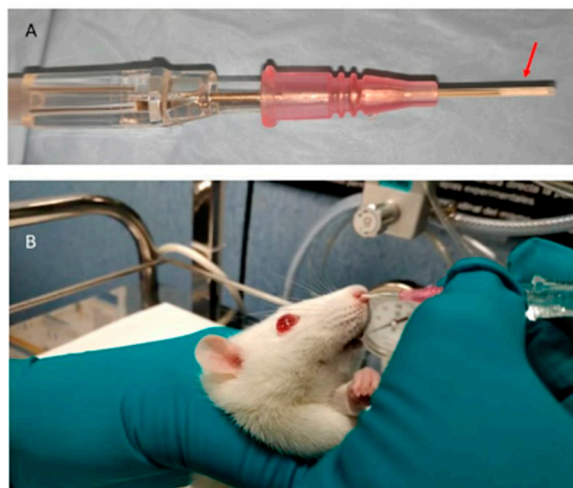


Figure 3. Microimplant (red arrow) placed inside the modified catheter (A). Intranasal administration of the implant to the animal (B).

After microimplant administration, *in vivo* images were acquired just post-administration (day 0) and at 1, 3, 7, 11, 14, 18, 21, and 28 days. SPECT scans were acquired in a U-SPECT6/E-class (MILabs, the Netherlands) using an ultrahigh resolution UHR-RM-1 mm multi-pinhole collimator. Rats were placed prone on the scanner bed under continuous anesthesia with isoflurane (2% in 100% O₂ gas) to acquire dynamic scans of the head in list mode format over 30 min. Following the SPECT acquisition, and without moving the animals, CT scans were performed to obtain anatomical information using a tube setting of 55 kV and 0.33 mA. All the SPECT images were reconstructed using the ¹²⁵I photopeak centered at 29 keV with a 20% energy window width and using a calibration factor to obtain the activity information (MBq/mL). Finally, attenuation correction was applied using the CT attenuation map. To obtain fully quantitative values (MBq), the system was calibrated using a point source prepared from [¹²⁵I]INa.

Studies were exported and analyzed using the PMOD software (PMOD Technologies Ltd., Adliswil, Switzerland), where fully three-dimensional fused SPECT/CT images were processed. The retention of radioactivity in the microimplant was calculated for each image as follows: a spherical volume of interest (VOI) containing the entire microimplant was drawn over SPECT images using the CT co-registered images as anatomical reference. Then, a semiautomatic delineation tool was used applying a predefined threshold of 1% of the maximum voxel value to obtain a new VOI that delimited the entire signal. Finally, the average value inside the VOI (MBq/mL) multiplied by the volume (mL) was calculated to estimate the amount of radioactivity retained in the microimplant. From these data, the corresponding ¹²⁵I decay correction based on the half-life ($T_{1/2}$) of ¹²⁵I and the time elapsed between the administration and the imaging was applied ($A = A_0 * e(-\ln(2) * t/T_{1/2})$). The percentage of the release was calculated as the inverse of the percentage of the retention detected in each image and considering the retention value in the 1 h post-administration image as the administered dose for each animal.

3. Results and Discussion

3.1. Reaction Optimization and Radiolabelling Yield

The radiolabeling yield was studied at different time intervals by radioTLC. Before taking a sample for radioTLC, the stirring speed was increased to be able to pipette a representative sample containing both a fraction of the solid (RISP) and the liquid in a suspension. Furthermore, after around 24 h, a solid precipitate could not be seen any more, and the suspension had a milky-turbid visual appearance. At 24 h, the labelling yield was around 50%, and it only increased marginally up to 72 h.

RISP iodination reaction was first tested in an Eppendorf tube. Although the tube was inverted several times every 2 h, a rather large part of the RISP was not in contact with the solution because it precipitated under reaction conditions and the contact of the solid with the iodination bead was not sufficient to get appropriate yields. Radiolabeling was then tested in a flat-bottom 5 mL glass vial that permitted continuous magnetic stirring at low speed for the overall reaction time (up to 72 h). Using the simple approach of combining a surface-based reaction on the iodination beads with a water-insoluble molecule such as RISP, we were able to carry out the radioiodination exchange reaction in suspension. Although the reaction yield was relatively low (around 25%), after extraction, centrifugation, and two consecutive washing steps, virtually all [^{125}I]I $^{-}$ was removed from the reaction mixture as determined by the radioTLC measurement of radioactivity in the different supernatants. The extraction and purification processes were optimized to maximize the purity of the final product, not the reaction yield.

RISP has previously been radiolabeled with ^{125}I [30], although by direct electrophilic substitution by oxidation with chloramine-T in an alcoholic solution of RISP. Strong oxidation with aggressive reagents such as chloramine-T might produce alterations in the molecule, and this requires a careful optimization of reaction conditions and times. In our hands, mild oxidation with iodination beads produced a smoother and more controllable reaction, albeit the final reaction yield was usually lower. Nonetheless, we decided to use a solid-supported electrophilic substitution and a final extraction step to maximize purity of ^{125}I -RISP and not reaction yield. In this way, using high specific activity [^{125}I]INa (≈ 629 GBq/mg), we were able to obtain >99% pure ^{125}I -RISP in sufficient amount to make PLGA microimplants containing radiolabeled RISP for in vivo imaging. Given the chemical structure of RISP, we might have considered radiolabeling it with fluorine-18 (a PET radionuclide with a half-life of 109.8 min) producing an identical molecule to the parent one. This is not only a very complex synthesis that has only been described in one paper thus far [31] (and never been used for in vivo imaging), but is also performed with an extremely short half-life radionuclide that could in no way be used for long-term release studies such as the ones presented here.

3.2. Quality Control Validation

As can be seen in Figure 4A, using iTLC SG strips developed in saline and stained with permanganate, the mixture of RISP and KI showed no interferences in TLC, and both species could be clearly resolved.

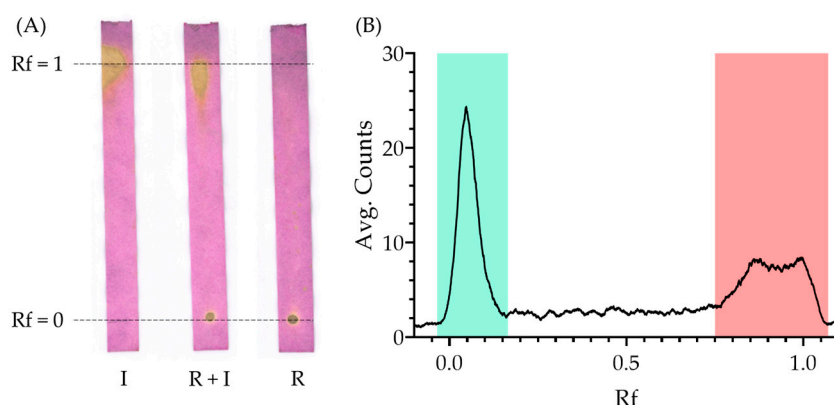


Figure 4. (A) Permanganate-stained TLC strips. RISP (R) remained at $R_f = 0$, while sodium iodide (I) advanced to the front ($R_f = 1$). The mixture of both compounds (R + I) showed that the mixture did not alter the individual results. (B) Representative radioTLC radiochromatogram of radiolabeled ^{125}I -RISP at 72 h, before purification.

When using radioactive samples for QC of RISP radiolabeling, both species were able to be properly resolved and identified (see a representative radioTLC chromatogram in Figure 4A,B).

3.3. *In Vivo* and *In Vitro* Release Studies

SPECT-CT images show the correct placement of the microimplant inside the nasal cavity of the animals (Figure 5), thus demonstrating the feasibility and accuracy of the administration procedure we developed. The sensitivity and resolution of MicroSPECT depends on the radionuclide used and the scanner, but it can be as low as 0.5 mm. Further details of the MicroSPECT/CT system were previously reported by Prieto et al. [32]. Longitudinal images acquired in all animals for around 4 weeks showed that the implants remained inside the nasal cavity for a long time (Figure 6). The amount of radioactivity in the microimplant progressively decreased over time (all data were corrected for the decay of ^{125}I and were hence comparable). When comparing the release of ^{125}I -RISP and $[^{125}\text{I}]\text{I}^-$, a clearly different pattern was seen with faster clearance of the former (Figure 6), probably due to its lipophilic nature. ^{125}I -RISP release reached around 45% by day 3 and then steadily but slowly increased up to 80% by day 21. $[^{125}\text{I}]\text{I}^-$ release was much slower, and it only accounted for 17% by day 12, and then it increased with a larger slope up to around 45% by day 21. Between 3 and 4 weeks after implantation, the implant moved from its original placement position towards the nostril, probably due to the progressive dissolving of the PLGA matrix (see Figure 6A at 28 days). The *in vivo* imaging technique used allowed us to even be able see this phenomenon.

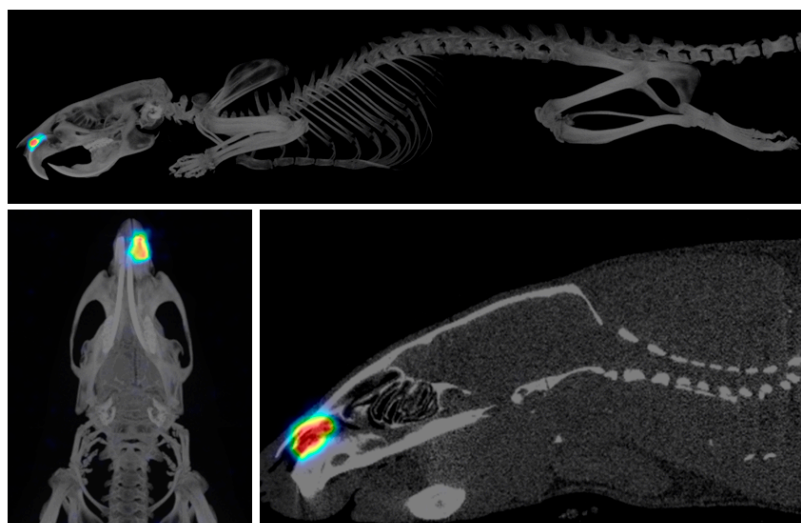


Figure 5. Fused MicroSPECT-CT images showing the location of the microimplant inside the nasal cavity. Hotter colours indicates higher concentration of radioactivity.

In vitro release studies of ^{125}I -RISP and $[^{125}\text{I}]\text{I}^-$ from the microimplants also showed a different pattern, although the different experimental conditions between *in vitro* and *in vivo* experiments figures were somewhat different (Figure 7). HPLC release studies of unlabeled RISP implants showed a fast release of RISP in the first 2 days (up to 65%) and then a very slow increase up to 80% by day 7.

All three methods (*in vivo* SPECT-CT imaging, *in vitro* radioactivity release studies, and HPLC release studies) showed a fast release of the drug in the first days and then a much steadier increase to reach a plateau-like situation. Release profiles are mostly comparable, but figures and slopes are different for each method, yet all three methods show that RISP can be released from our implants for a long time.

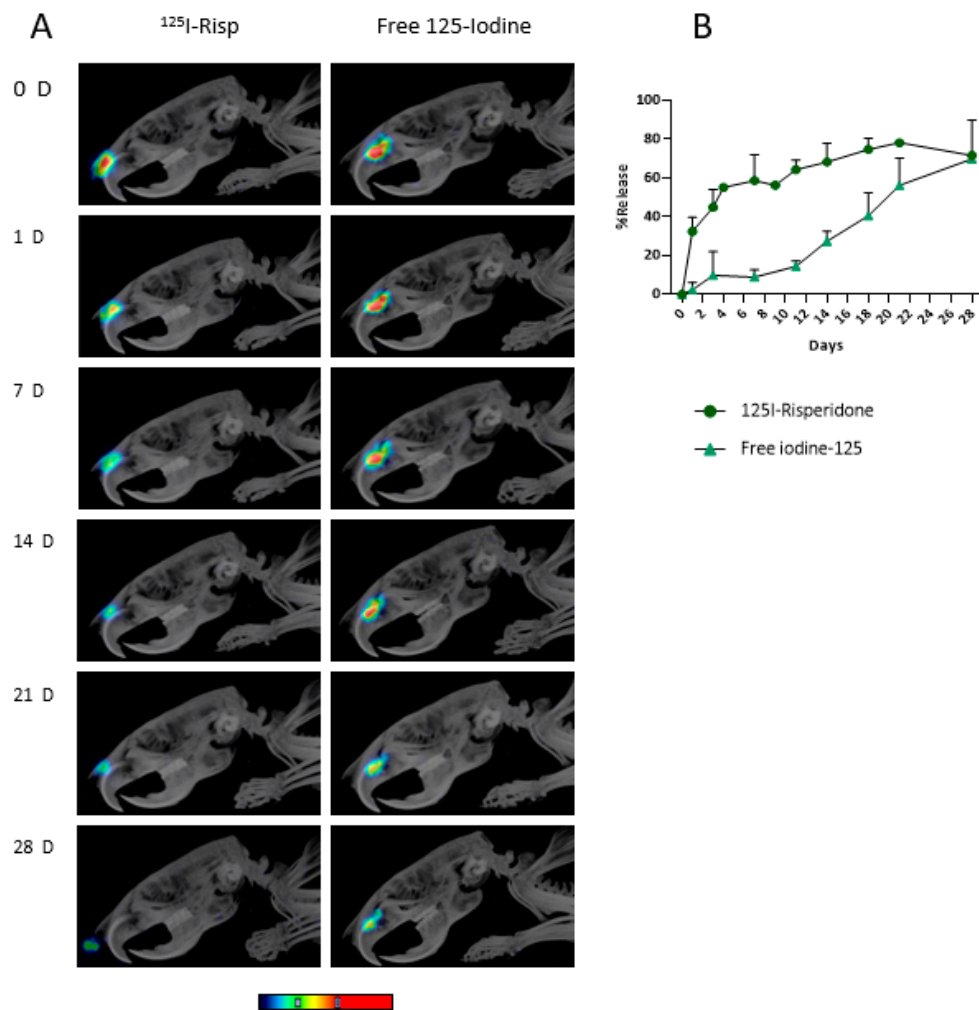


Figure 6. (A) Comparative release of radioactivity in vivo from ^{125}I -implants. MicroSPECT-CT images clearly show a progressive decrease in the amount of radioactivity in the nasal cavity over time, both for ^{125}I -RISP and $[\text{}^{125}\text{I}]\text{INa}$ implants. Hotter colours indicates higher concentration of radioactivity. The plot in (B) shows comparative quantitative values of radioactivity release as measured in the images on the left (mean \pm SD).

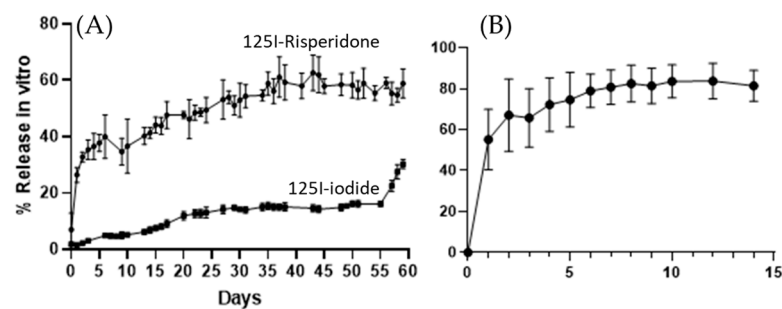


Figure 7. Radioactivity release in vitro from ^{125}I -implants are shown in (A), while (B) shows RISP release from implants as determined by HPLC (mean \pm SD).

The highly lipophilic drug used in these experiments was slowly but steadily released from the microimplants, while the release of a hydrophilic compound ($[\text{}^{125}\text{I}]\text{INa}$) took place at a slower rate. If both the lipophilic molecule and the ionic one would be equally trapped in the PLGA implant matrix, and their release would only depend on the progressive dissolution of the implants over time in vivo, quantitative values and release profiles of ^{125}I -RISP and $[\text{}^{125}\text{I}]\text{I}^-$ would be similar. Our data show that the lipophilic or hydrophilic nature

of the molecule of interest definitely conditions its release (as expected). Consequently, the dissolution of the implants would be responsible to some extent for the release of the loaded test molecule, but the specific physicochemical characteristics of the molecule under study and its interactions with the implant matrix are also of paramount importance, not only in *in vitro* experiments, but also *in vivo*, as shown by our images. The exact relationship between the release produced by dissolution of the implant and progressive release from the matrix are difficult to estimate for small ionic molecules (such as iodide) when a matrix as PLGA is used.

It is important to note that ^{125}I -RISP was not seen in the brain or any other part of the animal. The reason behind this could be the small amount of radioactivity used in each implant (just a few kBq, as compared to magnitudes in the order of MBq usually used for *in vivo* imaging in small animals). Furthermore, the passage of iodinated RISP through the nose to brain cribiform plate is unknown, and it might be different to some extent different to that of RISP, leading to a lower entrance into the brain. However, it is important to note that previous studies showed that intranasal RISP formulations showed enhanced drug uptake [33–35]. This work describes a new method for RISP radiolabeling and loading into intranasal microimplants. These implants have been designed to be implanted inside the nasal cavity to provide enhanced brain delivery of drugs for potential treatment of schizophrenia. Intranasal implants can revolutionize the treatment of chronic conditions affecting the central nervous system as they can provide sustained drug delivery and enhanced brain targeting. As mentioned previously, nasal stents and nasal drug eluting implants are currently been used to treat nasal polyps [24,36–39]. Accordingly, they are designed for localized drug delivery. Modifying this type of implant to provide sustained drug release into the brain can be used in the treatment of a wide range of chronic conditions. These devices are capable of providing prolonged drug delivery and, therefore, have potential to improve patient adherence to treatment [40–43]. This is especially important for schizophrenia treatment, as it has been reported that up to 75% of patients discontinue the treatment within the first year and a half [44]. Non-adherence to treatment has an enormous impact for this patient as it increases the risk of relapse, hospitalization, and even suicide rates [45–49]. Moreover, there is an obvious economic impact for healthcare systems. In the UK, it has been estimated that the cost of relapse per patient can be up to GBP 15,000 per year [50]. This figure is four times higher than the equivalent cost for non-relapse patients [51]. In addition, in order to improve patient compliance, nasal drug delivery will improve brain uptake, minimizing the risk of systemic exposure and potential side effects. Therefore, intranasal implants for the treatment of chronic conditions affecting the central nervous system offer multiple benefits to conventional treatment. However, before these systems can be used, *in vivo* testing is required. In the present work, we have shown potential alternatives to evaluate *in vivo* drug release using radiolabeled microimplants containing RISP.

4. Conclusions

To the best of our knowledge, this is the first study to describe the use of radiolabeled RISP for the development of intranasal implantable devices. This procedure can be used to evaluate drug release *in vitro* and *in vivo* in a simple way. This is especially important for *in vivo* drug delivery. We herein demonstrate the feasibility of this approach and its application to obtain high-resolution images of the release of the radiolabeled drug from the microimplants for more than one month. Furthermore, the possibility to accurately quantify *in vivo* the amount of the drug in the target, instead of simply measuring the concentration of the drug or its metabolites in the body fluids (i.e., blood, urine, etc.) as a result of the release, provides very valuable data for the development and fine-tuning of implantable long-term drug release devices. Future studies addressing the relationship between dosage of the number of therapeutic molecules in the brain and blood of the animals and the values quantitatively evaluated by imaging would further help clarify this point.

Author Contributions: Conceptualization, E.L. and I.P.; methodology, J.A.S., E.U., A.O., F.P. and G.Q.; animal handling and image acquisition, M.E.; image processing and analysis, M.C.; data analysis, I.P., E.L., J.D.-R. and M.C.; data curation, E.L., I.P. and J.D.-R.; writing—original draft preparation, J.A.S., I.P. and E.L.; writing—review and editing, I.P. and E.L.; funding acquisition, E.L. and I.P. All authors have read and agreed to the published version of the manuscript.

Funding: Fund for Education (Lembaga Pengelola Dana Pendidikan/LPDP), the Academy of Medical Sciences (SBF005\1011), MCIN/AEI/10.13039/501100011033, and the European Union NextGenerationEU/PRTR (Grant: RYC-2021-034357-I).

Institutional Review Board Statement: All the procedures involving animals were carried out in accordance with the guidelines of the European Communities Council Directive (2010/63/UE) and the Spanish legislation (Real Decreto 53/2013) and were approved by the Ethics Committee for Animal Experimentation of the University of Navarra (protocol CEEA/030-17[A]).

Informed Consent Statement: Not applicable.

Data Availability Statement: Data described in the manuscript, including all relevant images, are available from the corresponding author on reasonable request.

Acknowledgments: The authors would like to acknowledge the Academy of Medical Sciences (SBF005\1011) for the financial support and Ashland Specialties Ireland Limited for providing the Viatel PLGA polymer free of charge. Emilia Utomo would like to acknowledge the Indonesian Endowment Fund for Education (Lembaga Pengelola Dana Pendidikan/LPDP). Juan Domínguez-Robles would like to acknowledge the MCIN/AEI/10.13039/501100011033 and the European Union NextGenerationEU/PRTR for the following funding: grant RYC-2021-034357-I for the financial support to this work.

Conflicts of Interest: The authors declare no conflict of interest.

References

1. Quarterman, J.C.; Geary, S.M.; Salem, A.K. Evolution of drug-eluting biomedical implants for sustained drug delivery. *Eur. J. Pharm. Biopharm.* **2021**, *159*, 21–35. [[CrossRef](#)]
2. Stewart, A.S.; Domínguez-Robles, J.; Donnelly, R.F.; Larrañeta, E. Implantable polymeric drug delivery devices: Classification, manufacture, materials, and clinical applications. *Polymers* **2018**, *10*, 1379. [[CrossRef](#)]
3. Li, W.; Tang, J.; Lee, D.; Tice, T.R.; Schwendeman, S.P.; Prausnitz, M.R. Clinical translation of long-acting drug delivery formulations. *Nat. Rev. Mater.* **2022**, *7*, 406–420. [[CrossRef](#)]
4. Chappel, E. Implantable drug delivery devices. In *Drug Delivery Devices and Therapeutic Systems*; Elsevier: Amsterdam, The Netherlands, 2021; pp. 129–156.
5. Korelidou, A.; Domínguez-Robles, J.; Magill, E.; Eleftheriadou, M.; Cornelius, V.A.; Donnelly, R.F.; Margariti, A.; Larrañeta, E. 3D-printed reservoir-type implants containing poly(lactic acid)/poly(caprolactone) porous membranes for sustained drug delivery. *Biomater. Adv.* **2022**, *139*, 213024. [[CrossRef](#)]
6. Stewart, S.A.; Domínguez-Robles, J.; McIlorum, V.J.; Gonzalez, Z.; Utomo, E.; Mancuso, E.; Lamprou, D.A.; Donnelly, R.F.; Larrañeta, E. Poly(caprolactone)-based coatings on 3d-printed biodegradable implants: A novel strategy to prolong delivery of hydrophilic drugs. *Mol. Pharm.* **2020**, *17*, 3487–3500. [[CrossRef](#)]
7. Kumar, A.; Pillai, J. Implantable drug delivery systems. In *Nanostructures for the Engineering of Cells, Tissues and Organs*; Elsevier: Amsterdam, The Netherlands, 2018; pp. 473–511.
8. Abdelkader, H.; Fathalla, Z.; Seyfoddin, A.; Farahani, M.; Thrimawithana, T.; Allahham, A.; Alani, A.W.G.; Al-Kinani, A.A.; Alany, R.G. Polymeric long-acting drug delivery systems (ladds) for treatment of chronic diseases: Inserts, patches, wafers, and implants. *Adv. Drug Deliv. Rev.* **2021**, *177*, 113957. [[CrossRef](#)]
9. Picco, C.J.; Utomo, E.; McClean, A.; Domínguez-Robles, J.; Kurnia Anjani, Q.; Volpe-Zanutto, F.; McKenna, P.E.; Acheson, J.; Malinova, D.; Donnelly, R.F.; et al. Development of 3d-printed subcutaneous implants using concentrated polymer/drug solutions. *Int. J. Pharm.* **2022**, *631*, 122477. [[CrossRef](#)]
10. Simpson, S.M.; Widanapathirana, L.; Su, J.T.; Sung, S.; Watrous, D.; Qiu, J.; Pearson, E.; Evanoff, A.; Karunakaran, D.; Chacon, J.E.; et al. Design of a drug-eluting subcutaneous implant of the antiretroviral tenofovir alafenamide fumarate. *Pharm. Res.* **2020**, *37*, 83. [[CrossRef](#)]
11. Stewart, S.A.; Domínguez-Robles, J.; Utomo, E.; Picco, C.J.; Corduas, F.; Mancuso, E.; Amir, M.N.; Bahar, M.A.; Sumarheni, S.; Donnelly, R.F.; et al. Poly(caprolactone)-based subcutaneous implant for sustained delivery of levothyroxine. *Int. J. Pharm.* **2021**, *607*, 121011. [[CrossRef](#)]
12. Maturavongsadit, P.; Paravyan, G.; Kovarova, M.; Garcia, J.V.; Benhabbour, S.R. A New Engineering process of biodegradable polymeric solid implants for ultra-long-acting drug delivery. *Int. J. Pharm. X* **2021**, *3*, 100068. [[CrossRef](#)]

13. Lee, S.H.; Wan, Q.; Wentworth, A.; Ballinger, I.; Ishida, K.; Collins, J.E.; Tamang, S.; Huang, H.-W.; Li, C.; Hess, K.; et al. Implantable system for chronotherapy. *Sci. Adv.* **2021**, *7*, eabj4624. [[CrossRef](#)]
14. Myung, N.; Jin, S.; Cho, H.J.; Kang, H.-W. User-designed device with programmable release profile for localized treatment. *J. Control. Release* **2022**, *352*, 685–699. [[CrossRef](#)]
15. Lee, D.-H.; Torre Hernandez, J.M. de la The newest generation of drug-eluting stents and beyond. *Eur. Cardiol. Rev.* **2018**, *13*, 54. [[CrossRef](#)]
16. Domínguez-Robles, J.; Shen, T.; Cornelius, V.A.; Corduas, F.; Mancuso, E.; Donnelly, R.F.; Margariti, A.; Lamprou, D.A.; Larrañeta, E. Development of drug loaded cardiovascular prosthesis for thrombosis prevention using 3D printing. *Mater. Sci. Eng. C* **2021**, *129*, 112375. [[CrossRef](#)]
17. Spadaccio, C.; Chello, M.; Trombetta, M.; Rainer, A.; Toyoda, Y.; Genovese, J.A. Drug releasing systems in cardiovascular tissue engineering. *J. Cell. Mol. Med.* **2009**, *13*, 422–439. [[CrossRef](#)]
18. Khalaj, R.; Tabriz, A.G.; Okereke, M.I.; Douroumis, D. 3D printing advances in the development of stents. *Int. J. Pharm.* **2021**, *609*, 121153. [[CrossRef](#)]
19. Huang, C.; Lan, Y.; Chen, S.; Liu, Q.; Luo, X.; Xu, G.; Zhou, W.; Lin, F.; Peng, Y.; Ng, E.Y.K.; et al. Patient-specific coronary artery 3d printing based on intravascular optical coherence tomography and coronary angiography. *Complexity* **2019**, *2019*, 5712594. [[CrossRef](#)]
20. Bakola, V.; Karagkiozaki, V.; Tsiapla, A.R.; Pappa, F.; Moutsios, I.; Pavlidou, E.; Logothetidis, S. Dipyridamole-loaded biodegradable pla nanoplatfoms as coatings for cardiovascular stents. *Nanotechnology* **2018**, *29*, 275101. [[CrossRef](#)]
21. Martin, N.K.; Domínguez-Robles, J.; Stewart, S.A.; Cornelius, V.A.; Anjani, Q.K.; Utomo, E.; García-Romero, I.; Donnelly, R.F.; Margariti, A.; Lamprou, D.A.; et al. Fused deposition modelling for the development of drug loaded cardiovascular prosthesis. *Int. J. Pharm.* **2021**, *595*, 120243. [[CrossRef](#)]
22. Suhardi, V.J.; Bichara, D.A.; Kwok, S.J.J.; Freiberg, A.A.; Rubash, H.; Malchau, H.; Yun, S.H.; Muratoglu, O.K.; Oral, E. A Fully functional drug-eluting joint implant. *Nat. Biomed. Eng.* **2017**, *1*, 0080. [[CrossRef](#)]
23. Ma, X.; Gao, Y.; Zhao, D.; Zhang, W.; Zhao, W.; Wu, M.; Cui, Y.; Li, Q.; Zhang, Z.; Ma, C. Titanium implants and local drug delivery systems become mutual promoters in orthopedic clinics. *Nanomaterials* **2021**, *12*, 47. [[CrossRef](#)]
24. Parikh, A.; Anand, U.; Ugwu, M.C.; Feridooni, T.; Massoud, E.; Agu, R.U. Drug-eluting nasal implants: Formulation, characterization, clinical applications and challenges. *Pharmaceutics* **2014**, *6*, 249–267. [[CrossRef](#)]
25. Keller, L.-A.; Merkel, O.; Popp, A. Intranasal Drug Delivery: Opportunities and toxicologic challenges during drug development. *Drug Deliv. Transl. Res.* **2022**, *12*, 735–757. [[CrossRef](#)]
26. Utomo, E.; Domínguez-Robles, J.; Moreno-Castellanos, N.; Stewart, S.A.; Picco, C.J.; Anjani, Q.K.; Simón, J.A.; Peñuelas, I.; Donnelly, R.F.; Larrañeta, E. Development of intranasal implantable devices for schizophrenia treatment. *Int. J. Pharm.* **2022**, *624*, 122061. [[CrossRef](#)]
27. Formica, M.L.; Real, D.A.; Picchio, M.L.; Catlin, E.; Donnelly, R.F.; Paredes, A.J. On a highway to the brain: A review on nose-to-brain drug delivery using nanoparticles. *Appl. Mater. Today* **2022**, *29*, 101631. [[CrossRef](#)]
28. Aderibigbe, B. In situ-based gels for nose to brain delivery for the treatment of neurological diseases. *Pharmaceutics* **2018**, *10*, 40. [[CrossRef](#)]
29. Agrawal, M.; Saraf, S.; Saraf, S.; Dubey, S.K.; Puri, A.; Gupta, U.; Kesharwani, P.; Ravichandiran, V.; Kumar, P.; Naidu, V.G.M.; et al. Stimuli-responsive in situ gelling system for nose-to-brain drug delivery. *J. Control. Release* **2020**, *327*, 235–265. [[CrossRef](#)]
30. Saddar, E.; El-Tawoosy, M.; Motaleb, H.A. Preparation and biological evaluation of radioiodinated risperidone and lamotrigine as models for brain imaging agents. *J. Radioanal. Nucl. Chem.* **2014**, *301*, 189–196. [[CrossRef](#)]
31. Yuan, G.; Shoup, T.M.; Moon, S.-H.; Brownell, A.-L. A concise method for fully automated radiosyntheses of [18 F]jnj-46356479 and [18 F]fitm via cu-mediated 18 F-fluorination of organoboranes. *RSC Adv.* **2020**, *10*, 25223–25227. [[CrossRef](#)]
32. Prieto, E.; Irazola, L.; Collantes, M.; Ecay, M.; Cuenca, T.; Martí-Climent, J.M.; Peñuelas, I. Performance evaluation of a preclinical SPECT/CT system for multi-animal and multi-isotope quantitative experiments. *Sci. Rep.* **2022**, *12*, 18161. [[CrossRef](#)]
33. Patel, S.; Chavhan, S.; Soni, H.; Babbar, A.K.; Mathur, R.; Mishra, A.K.; Sawant, K. Brain targeting of risperidone-loaded solid lipid nanoparticles by intranasal route. *J. Drug Target.* **2011**, *19*, 468–474. [[CrossRef](#)]
34. Kumar, M.; Misra, A.; Babbar, A.K.; Mishra, A.K.; Mishra, P.; Pathak, K. Intranasal nanoemulsion based brain targeting drug delivery system of risperidone. *Int. J. Pharm.* **2008**, *358*, 285–291. [[CrossRef](#)]
35. Rukmangathen, R.; Yallamalli, I.M.; Yalavarthi, P.R. Formulation and biopharmaceutical evaluation of risperidone-loaded chitosan nanoparticles for intranasal delivery. *Drug Dev. Ind. Pharm.* **2019**, *45*, 1342–1350. [[CrossRef](#)]
36. Goshtasbi, K.; Abouzari, M.; Abiri, A.; Yasaka, T.; Sahyouni, R.; Bitner, B.; Tajudeen, B.A.; Kuan, E.C. Efficacy of steroid-eluting stents in management of chronic rhinosinusitis after endoscopic sinus surgery: Updated meta-analysis. *Int. Forum Allergy Rhinol.* **2019**, *9*, 1443–1450. [[CrossRef](#)]
37. Gadkaree, S.K.; Rathi, V.K.; Scangas, G.A.; Naunheim, M.R.; Metson, R. Use of corticosteroid-eluting sinus stents between 2012 and 2017. *JAMA Otolaryngol. Neck Surg.* **2019**, *145*, 90. [[CrossRef](#)]
38. Wang, C.; Yu, L.; Chu, X.; Wang, K.; Li, J.; Lai, Y.; Meng, C.; Wen, W.; Zhu, D.; Zhang, Y.; et al. Short-term postoperative efficacy of steroid-eluting stents for eosinophilic chronic rhinosinusitis with nasal polyps: A randomized clinical trial. *Int. Forum Allergy Rhinol.* **2022**. [[CrossRef](#)]

39. Huang, Z.; Zhou, B.; Wang, D.; Zang, H.; Zhang, H.; Wang, H.; Wang, S.; Cheng, L.; Li, J.; Wu, W.; et al. Comparison of bioabsorbable steroid-eluting sinus stents versus nasopore after endoscopic sinus surgery: A multicenter, randomized, controlled, single-blinded clinical trial. *Ear Nose Throat J.* **2022**, *101*, 260–267. [[CrossRef](#)]
40. Larrañeta, E.; Raghu Raj Singh, T.; Donnelly, R.F. Overview of the clinical current needs and potential applications for long-acting and implantable delivery systems. In *Long-Acting Drug Delivery Systems*; Elsevier: Amsterdam, The Netherlands, 2022; pp. 1–16.
41. Liaskoni, A.; Wildman, R.D.; Roberts, C.J. 3D printed polymeric drug-eluting implants. *Int. J. Pharm.* **2021**, *597*, 120330. [[CrossRef](#)]
42. Kar, A.; Ahamad, N.; Dewani, M.; Awasthi, L.; Patil, R.; Banerjee, R. Wearable and implantable devices for drug delivery: Applications and challenges. *Biomaterials* **2022**, *283*, 121435. [[CrossRef](#)]
43. Pons-Faudoa, F.P.; Ballerini, A.; Sakamoto, J.; Grattoni, A. Advanced implantable drug delivery technologies: Transforming the clinical landscape of therapeutics for chronic diseases. *Biomed. Microdevices* **2019**, *21*, 47. [[CrossRef](#)]
44. Higashi, K.; Medic, G.; Littlewood, K.J.; Diez, T.; Granstrom, O.; De Hert, M. Medication adherence in schizophrenia: Factors influencing adherence and consequences of nonadherence, a systematic literature review. *Ther. Adv. Psychopharmacol.* **2013**, *3*, 200–218. [[CrossRef](#)] [[PubMed](#)]
45. Haddad, P.M.; Brain, C.; Scott, J. Nonadherence with antipsychotic medication in schizophrenia: Challenges and management strategies. *Patient Relat. Outcome Meas.* **2014**, *5*, 43–62. [[CrossRef](#)] [[PubMed](#)]
46. Warriach, Z.I.; Sanchez-Gonzalez, M.A.; Ferrer, G.F. Suicidal behavior and medication adherence in schizophrenic patients. *Cureus* **2021**, *13*, e12473. [[CrossRef](#)]
47. Moges, S.; Belete, T.; Mekonen, T.; Menberu, M. Lifetime relapse and its associated factors among people with schizophrenia spectrum disorders who are on follow up at comprehensive specialized hospitals in amhara region, ethiopia: A cross-sectional study. *Int. J. Ment. Health Syst.* **2021**, *15*, 42. [[CrossRef](#)] [[PubMed](#)]
48. Li, G.; Keenan, A.; Daskiran, M.; Mathews, M.; Nuamah, I.; Orman, C.; Joshi, K.; Singh, A.; Godet, A.; Pungor, K.; et al. Relapse and treatment adherence in patients with schizophrenia switching from paliperidone palmitate once-monthly to three-monthly formulation: A retrospective health claims database analysis. *Patient Prefer. Adherence* **2021**, *15*, 2239–2248. [[CrossRef](#)]
49. Fernández-Miranda, J.J.; Díaz-Fernández, S.; López-Muñoz, F. Effectiveness of more personalized, case-managed, and multicomponent treatment for patients with severe schizophrenia compared to the standard treatment: A ten-year follow-up. *J. Pers. Med.* **2022**, *12*, 1101. [[CrossRef](#)] [[PubMed](#)]
50. Pennington, M.; McCrone, P. The cost of relapse in schizophrenia. *Pharmacoeconomics* **2017**, *35*, 921–936. [[CrossRef](#)]
51. Almond, S.; Knapp, M.; Francois, C.; Toumi, M.; Brugha, T. Relapse in schizophrenia: Costs, clinical outcomes and quality of life. *Br. J. Psychiatry* **2004**, *184*, 346–351. [[CrossRef](#)]

Disclaimer/Publisher’s Note: The statements, opinions and data contained in all publications are solely those of the individual author(s) and contributor(s) and not of MDPI and/or the editor(s). MDPI and/or the editor(s) disclaim responsibility for any injury to people or property resulting from any ideas, methods, instructions or products referred to in the content.